

SYNCHROTRON CONSTRAINTS ON A HYBRID COSMIC-RAY AND THERMALLY-DRIVEN GALACTIC WIND

BY JOHN E. EVERETT^{1,2,3}, QUINTIN G. SCHILLER², ELLEN G. ZWEIBEL^{1,2,3}

Draft version March 2, 2022

ABSTRACT

Cosmic rays and magnetic fields can substantially impact the launching of large-scale galactic winds. Many researchers have investigated the role of cosmic rays; our group previously showed that a cosmic-ray and thermally-driven wind could explain soft X-ray emission towards the center of the Galaxy. In this paper, we calculate the synchrotron emission from our original wind model and compare it to observations; the synchrotron data shows that earlier assumptions about the launching conditions of the wind must be changed: we are required to improve that earlier model by restricting the launching region to the domain of the inner “Molecular Ring”, and by decreasing the magnetic field strength from the previously assumed maximum strength. With these physically-motivated modifications, we find that a wind model can fit both the radio synchrotron and the X-ray emission, although that model is required to have a higher gas pressure and density than the previous model in order to reproduce the observed X-ray emission measure within the smaller ‘footprint’. The drop in magnetic field also decreases the effect of cosmic-ray heating, requiring a higher temperature at the base of the wind than the previous model.

Subject headings: ISM:outflows – ISM:cosmic rays – ISM:magnetic fields – Galaxy:kinematics – Galaxy:evolution – Xrays:diffuse background

1. INTRODUCTION

The possibility of thermal-pressure driven outflows on galactic scales has been considered for some time (see, e.g., Veilleux et al. 2005, and references therein). Somewhat less well-known, however, is the possibility that cosmic rays and magnetic fields can also help drive outflows: if, as commonly assumed and even sometimes observed, magnetic-field pressure and cosmic-ray pressure are in approximate equipartition with the hot-gas thermal pressure within galactic disks (e.g., Duric 1990; Pohl 1993; Heiles 1996; Zweibel & Heiles 1997; Webber 1998; Beck 2001; Cox 2005), these sources of energy will be important in large-scale outflows in more quiescent galaxies, such as perhaps our Milky Way. Understanding and constraining the dynamics and observational constraints on such kpc-scale galactic outflows is the main aim of the present paper.

The possibility of a kpc-scale outflow from the Milky Way has been studied for over three decades (e.g., Ipavich 1975; Breitschwerdt et al. 1987, 1991, 1993; Bland-Hawthorn & Cohen 2003; Breitschwerdt 2003; Veilleux et al. 2005), including work on the observational effects of such an outflow (e.g., Lerche & Schlickeiser 1982; Jokipii & Morfill 1987; Reich & Reich 1988a; Pohl & Schlickeiser 1990; Bloemen 1991; Bloemen et al. 1993; Breitschwerdt & Schmutzler 1994; Zirakashvili et al. 1996; Ptuskin et al. 1997; Breitschwerdt et al. 2002). Bland-Hawthorn & Cohen (2003) showed possible evidence for such an outflow in X-ray, infrared, and radio observations, along with models of a bipolar structure. In Everett et al. (2008, hereafter Paper I), we continued this work by building a wind model powered by both cosmic-ray pressure and thermal-gas pressure. In such winds, cosmic rays yield some of their energy to Alfvén waves on the magnetic field

via the “Streaming Instability” (Kulsrud & Pearce 1969) which are then damped to deliver energy and momentum to the thermal gas. We applied that model to observations of excess diffuse X-ray emission towards the inner Galaxy (Snowden et al. 1995, 1997; Almy et al. 2000). Paper I built especially on Breitschwerdt et al. (1991), but with the following modifications: the wind is launched from a restricted range of Galactocentric radii (an annulus in the inner Galaxy), originates at the Galactic midplane with a vertical magnetic field, and (as indicated by our analytical work) the cosmic-ray generated Alfvén waves are completely damped, subsequently heating the gas. This model fit the longitude-averaged X-ray emission observed with *ROSAT* near 0.65 keV and 0.85 keV with χ^2 values a factor of two smaller than the previous static model (Almy et al. 2000), while simultaneously yielding pressure and density parameters approximately equal to those already inferred for hot gas near this region in the inner Milky Way (c.f., Ferrière 2001, hereafter, F01).

The above initial model (reviewed in §2) was derived solely from a fit to the soft X-ray emission and made several assumptions that bear continued examination. In this paper, we test the wind model further by comparing calculations of the synchrotron emission from the wind to 408-MHz all-sky surveys towards the center of the Galaxy: radio-synchrotron observations are an important constraint on a cosmic-ray and thermal-gas pressure-driven outflow, given the dependence on both the cosmic-ray pressure (albeit through the uncertain and energy-dependent ratio of cosmic-ray electrons to protons) and the magnetic field strength, both of which are crucial in our model. Many groups have worked to understand the distribution of synchrotron emission in the halo (F01; Beuermann et al. 1985; Reich & Reich 1988a,b; Broadbent et al. 1990; Strong et al. 2000; Reich et al. 2004; Sun et al. 2008; de Oliveira-Costa et al. 2008; Reich & Reich 2008; Waelkens et al. 2009), but more work is needed to understand the role of cosmic-ray advection into the halo via a wind and the subsequent cooling of cosmic-ray electrons via

everett@physics.wisc.edu

¹ University of Wisconsin–Madison, Department of Astronomy

² University of Wisconsin–Madison, Department of Physics

³ Center for Magnetic Self-Organization in Laboratory and Astrophysical Plasmas

inverse-Compton and synchrotron cooling (although we note that the cosmic-ray propagation code GALPROP has an approximate Galaxy-wide wind model with a constant velocity gradient; see, e.g., Porter et al. 2008, and references therein).

In this work, we build a model of the synchrotron emission of a large-scale wind launched from an annulus in the inner Galaxy, taking into account synchrotron and inverse-Compton cooling and the full velocity gradient in the wind; this work is detailed in §3. We also present predictions for the synchrotron spectral index, but note the possibly strong importance of foreground synchrotron emission. By comparing the observed synchrotron emission to that calculated for the model of Paper I, the observations can then be used to examine two assumptions made in Paper I: the radial range on the Galactic disk where the wind is launched and the magnetic field strength.

The calculated synchrotron emission will show that the wind model of Paper I overpredicts the observed radio emission; the observed synchrotron emission is therefore a strong constraint on the wind model. As outlined above, we then consider if it is possible for a modified wind model to fit the observations; these possibilities are explained in §4. First, the wind may have a thinner footprint than the $\Delta R = 3$ kpc width used in Paper I (§4.1); this is suggested by observations of the “5 kpc Molecular Ring” (Jackson et al. 2006, B. Benjamin, private communication). Second, the magnetic field strength within the wind might be lower than the value of $7.8 \mu\text{G}$ used in Paper I (§4.2). Third, the cosmic-ray electron-to-proton ratio may be different towards the center of the Galaxy, although we find it unnecessary to invoke this, given other, more physically motivated and astrophysically constrained modifications to the model (§3.1). (We also modify the χ^2 fit parameter to avoid biases due to assumptions about X-ray absorption in §4.3.) Then, in §4.4, we present the best-fit wind model that addresses both the soft X-ray and synchrotron observations, and compare this model to that of Paper I. Finally, we discuss the results in §5.

2. THE HYBRID COSMIC-RAY AND THERMALLY-DRIVEN WIND MODEL

Before we outline our model of synchrotron emission from the wind, we first review the wind model from Paper I. This model was motivated by observations of the inner Milky Way, where an excess of $T \sim 3 \times 10^6$ K, X-ray emitting gas has been observed with a scaleheight of ~ 2 kpc (Snowden et al. 1995, 1997; Park et al. 1997, 1998; Almy et al. 2000). Some attempts had been made (Snowden et al. 1997; Almy et al. 2000) to fit this emission with static gas distributions, as the gas pressure of the plasma is insufficient, on its own, to drive a wind from the Milky Way. Our group asked whether cosmic-ray momentum and energy could be communicated, via the “Streaming Instability” (Wentzel 1968; Kulsrud & Pearce 1969; Kulsrud & Cesarsky 1971), to the thermal gas, and hence be used to launch a wind. We were not the first to ask this question; building on much past research into the power of cosmic rays to affect gas dynamics and help drive a wind (e.g., Ipavich 1975; Skilling 1975; Bloemen 1991; Breitschwerdt et al. 1991, 1993; Breitschwerdt & Schmutzler 1994; Zirakashvili et al. 1996; Ptuskin et al. 1997; Zirakashvili & Völk 2006), we assembled a 1D hydrodynamical model of a cosmic-ray pressure and thermal-pressure driven wind. The equations for this wind model are reviewed in the Appendix.

The model of Paper I differed from previous models in that we concentrated solely on understanding the enhanced X-ray emission towards the inner Milky Way. Taking the hypothesis that the emission is centered on the Galactic Center (Almy et al. 2000), we limited the maximum radial extent of the wind to 4.5 kpc in Galactocentric radius. We assumed the wind was launched from the midplane of the Galaxy; the wind then flows vertically within flowtubes with cross-sectional area given by a simple analytic form with a characteristic expansion height that is a free parameter (as in Breitschwerdt et al. 1991). We set the initial cosmic-ray pressure and magnetic field strength to the values inferred from synchrotron observations at the Galaxy’s midplane (F01), assuming a vertical magnetic field. The initial gas pressure and density at the Galactic midplane, which are relatively poorly known, were left as free parameters. In early tests, we found that for fiducial values of all these parameters, winds could not escape from the very inner portion of the Galaxy ($R \lesssim 1.5$ kpc), so we hypothesized an annular geometry, with the wind only occupying a thick ring from 1.5 kpc to 4.5 kpc. (This inner region without a wind may correspond to the transition from a wind to an X-ray emitting atmosphere of gravitationally confined supernova-heated gas hypothesized in more massive spheroids by Binney 2009).

Values for the three free parameters (gas pressure & density at the midplane, and the scale-height of flowtube expansion) were then found by fitting the predicted X-ray emission of the wind to the observed emission in *ROSAT*’s R4 and R5 bands; the wind was found to provide a significantly improved fit (by a factor of two in χ^2) over the static polytrope of Almy et al. (2000). In addition, the gas pressure and density values that were found in this process were plausible for the inner Galaxy (see Table 1). Finally, the power required to launch this wind was approximately a factor of two higher than the estimated supernova power, which was plausible given the many approximations of the theory, but possibly indicated that further model refinement and/or constraints were necessary. Despite the clear simplicity of this approximate model, such a cosmic-ray pressure- and thermal-gas pressure-driven wind within our Galaxy seemed to fit the observations well.

X-ray observations alone do not uniquely determine the structure of the wind; comparisons of the model to synchrotron data allow a natural and complimentary check. We outline the synchrotron-emission calculation and compare the predicted emission to the observations in §3. The predicted synchrotron emission is larger than what is observed, so we vary other aspects of the wind model in §4. The resulting best-fit model provides nearly as good a fit to the X-ray observations as the original model of Paper I and is more consistent with other known aspects of galactic structure.

3. CALCULATING THE SYNCHROTRON EMISSION

Given the above magnetic field and cosmic-ray density (defined by the wind model presented in Paper I), the synchrotron intensity along a line of sight can be integrated via equation (3.20) from Ginzburg & Syrovatskii (1965):

$$I_\nu = \frac{\sqrt{3}e^3}{m_e c^2} \int n(E_e, \mathbf{r}, \mathbf{k}) B(r) \sin \theta \left(\frac{\nu}{\nu_c} \int_{\nu/\nu_c}^{\infty} K_{5/3}(\eta) d\eta \right) dE_e dr, \quad (1)$$

where e is the electron charge, m_e is the electron mass, and c is the speed of light. $n(E_e, \mathbf{r}, \mathbf{k})$ is the cosmic-ray electron density, which is a function of cosmic-ray electron energy,

E_e , position, \mathbf{r} , and direction, \mathbf{k} . $K_{5/3}$ is the Bessel function of the second kind, $B(\mathbf{r})$ is the magnetic field strength as a function of position, θ is the angle between \mathbf{B} and \mathbf{k} , ν is the observation frequency, and ν_c is defined by:

$$\nu_c \equiv \frac{3eB_{\perp}}{4\pi m_e c} \left(\frac{E_e}{m_e c^2} \right)^2. \quad (2)$$

For evaluating and integrating the full synchrotron intensity equation, $n(E_e, \mathbf{r}, \mathbf{k})$ is required throughout the wind: we calculate $n(E_e, \mathbf{r}, \mathbf{k})$ by assuming a given initial electron distribution (§3.1), and accounting for the integrated inverse-Compton, synchrotron, and adiabatic losses (§3.2) as the wind is launched from the disk. After we give the details for the calculation, below, we briefly outline the convergence tests the code has passed (§3.3), define the backgrounds (§3.4) and foregrounds (§3.5) that must be included, and show the prediction for synchrotron emission from the wind in §3.6.

3.1. The Galactic Midplane Cosmic-Ray Electron Spectrum

The wind equations for this model consider both the thermal gas and cosmic rays as fluids. To model the synchrotron radiation of the cosmic-ray electrons, we have to model in more detail the cosmic-ray electron spectrum with energy. To do this, we first take, as a typical cosmic-ray electron spectrum, the electron spectrum observed at the Galactic midplane at the Sun's position (F01). As in F01, we use the normalization from Figure 6 of Webber (1983) where, at 2.3 GeV, $dn/dE = 17.3 \text{ m}^{-2} \text{ sec}^{-1} \text{ ster}^{-1} \text{ GeV/nucleon}^{-1}$. We then convert this result from the Sun's position to a Galactocentric radius of $R = 3.5 \text{ kpc}$ by multiplying that local cosmic-ray electron flux by a factor of 2.4, as derived in Equation 11 of F01. This factor comes from fitting the variation of synchrotron radiation in the Galactic midplane as observed by Beuermann et al. (1985).

For consistency, we also use the cosmic-ray electron-spectrum power-law of $\gamma = 2.5$ from F01. We assume that this cosmic-ray electron spectrum is constant at the Galactic midplane, and constant over time, evolving only with height in the wind due to cooling. Of course, if the CR e^-/p ratio changes towards the center of the Galaxy from that observed locally, such a change would produce a directly proportional change in the synchrotron intensity. We point out that a different input spectrum may be possible, as Strong et al. (2004a) find that their Galactic propagation models imply a different electron-injection spectrum from that used in Paper I or in the present work. Such uncertainties represent a large area of parameter space that adds more complexity via another free parameter, and so we choose instead to retain the present spectrum, based on local measurements. Our synchrotron results could easily be scaled to lower or higher CR e^- densities; as we will see in §4, this is not necessary to fit the observed synchrotron emission.

We note briefly that the above procedure is similar to that we used to estimate the cosmic-ray proton pressure at the base of the wind in Paper I; as in F01, we have assumed that the local cosmic-ray proton to cosmic-ray electron ratio applies also to the area at the base of this wind. This is mentioned further in §4.4. The electron-to-proton ratio is set to 1:50; one could assume various ratios up to 1:100, perhaps, but assuming 1:50 should force relatively strong constraints on the wind model when comparing to radio synchrotron emission.

3.2. Cooling the Cosmic-Ray Electrons

To include the effects of inverse-Compton cooling on the cosmic-ray electrons, we use the representation of the interstellar radiation field (ISRF) that has been developed for use with the GALPROP code (available at <http://galprop.stanford.edu/>; see Strong & Moskalenko 1998; Strong et al. 2000, 2004a; Porter & et al. 2005; Porter et al. 2008)⁴. In their model, the ISRF is given as a function of wavelength on a regularly spaced grid in Galactocentric radius and height above the plane: the radial grid has 41 elements in Galactocentric radius, starting at 0.25 kpc and spaced at 0.5 kpc increments. The height grid starts at $z = -5 \text{ kpc}$ and is spaced in increments of 0.1 kpc, in 101 steps, to $z = 5 \text{ kpc}$. The ISRF photon field is then converted to $f_{\gamma}(\omega)$, the background photon distribution (see Appendix C, Strong & Moskalenko 1998) via the definition:

$$U_{\text{ph}} = m_e c^2 \int \omega^3 f_{\gamma}(\omega) d\omega, \quad (3)$$

where U_{ph} is the energy density of the ISRF, ω is the photon frequency, and γ is the electron Lorentz factor. With the ISRF photon distribution, we can then write the equation for inverse-Compton cooling (see, again, Appendix C of Strong & Moskalenko 1998, and references therein) as:

$$\left(\frac{dE}{dt} \right)_{\text{IC}} = \frac{\pi r_e^2 m_e c^3}{2\gamma^2 \beta} \int_0^{\infty} f_{\gamma}(\omega) [S(\gamma, \omega, k^+) - S(\gamma, \omega, k^-)], \quad (4)$$

where

$$S(\gamma, \omega, k) = \omega \left\{ \left(k + \frac{31}{6} + \frac{5}{k} + \frac{3}{2k^2} \right) \ln(2k+1) - \frac{11}{6}k - \frac{3}{k} + \frac{1}{12(2k+1)} + \frac{1}{12(2k+1)^2} + Li_2(-2k) \right\} - \gamma \left\{ \left(k + 6 + \frac{3}{k} \right) \ln(2k+1) - \frac{11}{6}k + \frac{1}{4(2k+1)} - \frac{1}{12(2k+1)^2} + 2Li_2(-2k) \right\}, \quad (5)$$

and where $Li_2(\dots)$ denotes the dilogarithmic function (the polylogarithm with $n=2$; see Abramowitz & Stegun 1972), $\beta = v/c$ for the cosmic-ray electrons, and $k^{\pm} \equiv \omega\gamma(1 \pm \beta)$. For completeness, we note that the full application of this formula to the production of γ -ray emission requires the consideration of anisotropic scattering (see Moskalenko & Strong 2000); in the present case of simple cooling, where we need only the absolute power emitted, the anisotropic nature of the radiation field is not important.

We also include the energy loss from synchrotron cooling:

$$\left(\frac{dE}{dt} \right)_{\text{synch}} = -\frac{32}{9} \pi r_e^2 c U_B \gamma^2 \beta^2. \quad (6)$$

Adiabatic cooling is already included via the hydrodynamic cosmic-ray model of the wind.

In summary, then, the hydrodynamic wind model includes the adiabatic cooling, and then a separate synchrotron-modeling program implements the energy-dependent inverse-

⁴ The ISRF data file is http://galprop.stanford.edu/FITS/MilkyWay_DR0.5_DZ0.1_DPFI10_RMAX20_ZMAX5_galprop_format.fits.gz, downloaded on September 23rd, 2008 from http://galprop.stanford.edu/web_galprop/galprop_home.html.

Compton (Eq. 4) and synchrotron (Eq. 6) cooling losses for the energy resolved electron distribution.

To calculate the effect of these cooling terms, the Δt for each discrete vertical step of the wind is calculated from the velocity profile, and then simply multiplied by the above cooling rate at every step. The inverse-Compton and synchrotron cooling do substantially impact the energy density of the cosmic-ray electrons. It is important to note, however, that neither process impacts the cosmic-ray protons, which are the source of momentum for driving winds; cosmic-ray electrons, with a number density only approximately 2% that of the cosmic-ray protons, do not contribute significantly to the cosmic-ray pressure. So, in this case, when we consider cosmic-ray electrons as a separate component, and cool those electrons in an already defined wind model, that cooling does not impact the wind model (such as the mass outflow rate and velocities achieved, for instance).

Following the calculation of the local electron spectrum, the local intensity is calculated and then integrated numerically on lines of sight through the wind; synchrotron self-absorption does not play a role in the Galaxy for $\nu \gtrsim 50$ MHz, so it is neglected here. This calculation is carried out over a grid in Galactic longitude & latitude. We then average the emission over longitude (as done previously for the comparison with the soft X-ray emission) and plot it as a function of latitude to compare with observations.

How do the various cooling terms compare? We have found that inverse-Compton and synchrotron cooling of cosmic-ray electrons dominate adiabatic cooling by a factor or ~ 10 near $z \sim 500$ pc, but that adiabatic cooling achieves parity around $z \sim 2$ kpc above the Galactic midplane, reaching a maximum in relative strength (2.5 times the total of inverse-Compton and synchrotron cooling) at approximately 5 kpc; above this height, adiabatic cooling decreases again to become approximately equal to both inverse-Compton and synchrotron cooling (we have calculated the above energy losses over the entire electron-energy distribution that we consider, from $\sim 10^{-3}$ GeV to 100 GeV). The models also demonstrate that inverse-Compton cooling is more important than synchrotron cooling by approximately an order of magnitude near $R = 3.5$ kpc. Also, we have found that Klein-Nishina effects are significant at 408 MHz, with total inverse-Compton cooling dropping to 65% of that calculated from the non-relativistic approximation.

3.3. Testing the Synchrotron Code

Before running the full synchrotron calculation with cooling, we developed an initial version of the code that assumed a constant (non-cooling) cosmic-ray electron population with a power-law index of 2.7. This code was checked against analytic estimates for the synchrotron emission along various lines of sight, and was used to check convergence of the flux integration with various line-of-sight stepsizes; the algorithm reproduced the analytical results within $\sim 5\%$.

We have also tested the synchrotron code by checking for convergence in a wide range of parameters used within the code: for instance, we have checked that the code converges when using a larger number of electron bins in the CR-electron spectrum, smaller vertical step-sizes in the cooling calculation, and higher resolution in all numerical integrals. All of the higher-resolution studies yield less than 5% differences in the predicted synchrotron emission. This algorithm also reproduces (within 3%) the result of Ferrière (2001) for the synchrotron emission of the Galactic midplane. Finally,

the code can also be run in a “static halo” mode without any cooling terms or flow velocities; those runs reproduced the expected flat spectral indices to approximately 1 part in 10^4 .

3.4. Synchrotron Backgrounds

Before comparing to observations, we must also account for the various backgrounds in the data, adding those components to the wind model’s synchrotron emission. As shown in Reich et al. (2004), and in more detail in Reich & Reich (2008), the observed brightness temperature (T_{OBS}) can be understood as the sum:

$$T_{\text{OBS}} = T_{\text{GAL}} + T_{\text{CMB}} + T_{\text{EXG}} + T_{\text{OFF}} \quad (7)$$

where

$$T_{\text{GAL}} = \text{intrinsic Galactic brightness temperature} \quad (8)$$

$$T_{\text{CMB}} = \text{cosmic microwave background} = 2.73 \text{ K} \quad (9)$$

$$T_{\text{OFF}} = \text{zero-level error} \quad (10)$$

$$T_{\text{EXG}} = \text{unresolved extragalactic sources} \quad (11)$$

We calculate the extragalactic contribution from the formula (see Reich et al. 2004, and references therein):

$$T_{\text{EXG}} = 30 \text{ K} \left(\frac{\nu}{178 \text{ MHz}} \right)^{-2.9} \quad (12)$$

and take T_{OFF} from Reich et al. (2004).

3.5. A Strong Local Synchrotron Foreground?

After adding in all of these background components to the model, we were intrigued to find a relatively constant level of high-latitude (at $|b| \gtrsim 40^\circ$) emission that remained unexplained, and would not be explained by the wind emission, which would only be important up to $|b| \sim 20^\circ$. The Galactic synchrotron model of Beuermann et al. (1985) also does not address this component; they only fit the synchrotron emission at low latitudes ($b \lesssim \pm 3^\circ$). So, it seems that the nature and origin of this high-latitude component are not well understood, and have not been accounted for in the “standard model” of Beuermann et al. (1985). From the near constancy of the high-latitude emission, from the recent evidence for a relatively local synchrotron emission component (Fleishman & Tokarev 1995; Roger et al. 1999; Wolleben 2007; Sun et al. 2008, and W. Reich (personal communication)), and from our own (brief) analysis of the 408 MHz to 1420 MHz spectral indices which seem to indicate a temperature spectral index near $\beta \sim 2.75$, we conservatively hypothesize that this high-latitude emission at $|b| \gtrsim 40^\circ$ is local, and therefore is a foreground Galactic component that should be accounted for separately when comparing the wind to the observed emission. This is important, as the wind model should not predict a larger synchrotron emission than is observed in any part of the sky; the presence of a local synchrotron foreground makes this, of course, more difficult for the model, which is therefore even more restricted by the observations.

In addition, as we will show later, these foreground components are also essential in comparing the synchrotron spectral index of models to observations, and so highlight the importance for a more global model of the Galactic synchrotron emission (perhaps like that in GALPROP, but including a more general wind model; see Strong et al. 2004a; Sun et al. 2008; Waelkens et al. 2009). *It is also important to emphasize that if this emission is local, then the synchrotron halo of*

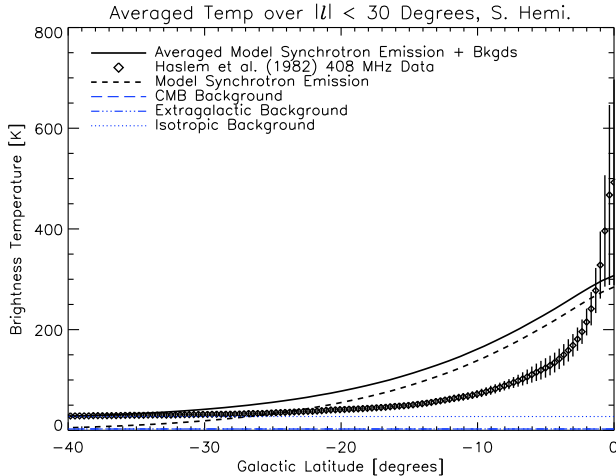


FIG. 1.— The 408MHz synchrotron brightness temperature predicted by the wind model presented in Paper I. The predicted synchrotron brightness significantly overpredicts the observed emission by approximately a factor of two.

the Milky Way, as inferred from *Beuermann et al. (1985)*, is substantially overestimated (W. Reich, personal communication).

3.6. Synchrotron Emission from the Wind Model of Paper I

With all of these components added in, we calculate the absolute intensity of synchrotron emission at 408MHz with the original wind model (as presented in Paper I) plus background and foreground emission. We find that that model *substantially* over-produces synchrotron emission above the plane, as shown in Figure 1. The wind does not dominate the synchrotron emission in the disk, but, crucially, falls off too slowly with height, violating observational constraints strongly near $b \sim 6^\circ$. As such, the original model in Paper I is not in agreement with the observations, and must be discarded as a “best-fit” to the combined observations. Clearly, either the assumed magnetic field is too high, the wind volume is too large, or the cosmic-ray electron density is too high to fit the observed synchrotron emission.

We now ask: is there a simple way for the model to be brought into closer agreement with both the soft X-ray and synchrotron observations, while at the same time, improving the basic assumptions of the model of Paper I?

4. CAN AN IMPROVED WIND MODEL FIT BOTH X-RAY AND SYNCHROTRON OBSERVATIONS?

We now consider two physically-motivated possibilities for updating the previously assumed launch parameters of the wind as well as one modification for making more robust comparisons between the model and X-ray data. These modifications are motivated by the overprediction of synchrotron emission in the original model but also incorporate current thinking about the structure of the inner Galaxy. We then check whether such changes may help bring a cosmic-ray and thermally-driven wind model in agreement with the observations, and consider the effect of these modifications on wind driving.

4.1. A Wind From the “Molecular Ring”

As mentioned in the introduction, Paper I had included the assumption that the wind was launched from a range of Galactocentric radii, from 1.5 to 4.5 kpc. The inner radius was the minimum radius at which a wind can be launched in the gravitational potential of the inner Galaxy. The observed edge of the soft X-ray emission at $l \sim \pm 30^\circ$ set the outer radius of the wind. In the course of that previous work, it was suggested by R. Benjamin (personal communication) that the wind might more naturally be considered to be launched from the “5 kpc Molecular Ring” (e.g., Jackson et al. 2006), which is much thinner, with a range of Galactocentric radii of approximately $\Delta R \sim 1$ to 1.5 kpc. This “5 kpc Molecular Ring” is home to the largest level of star formation in our Galaxy, and so is a reasonable location for a wind launched by hot gas and cosmic rays. So, in this work, we attempt to fit the X-ray emission with a wind that covers only 1 kpc on the Galactic disk, from $R = 3.5$ kpc to 4.5 kpc. (This thinner wind may hint at a more massive central Galactic bulge; it also increases the importance of any X-ray emission from static gas in the bulge, which we do not include in the model here.)

For future development of the model, we note that the “Molecular Ring” is, of course, not observed to be uniform in azimuth, and so an even more realistic assumption for launching would include a covering fraction of the wind within this annulus. This would require, however, development of a more detailed model of the lateral force balance as a function of height off the surface of the disk, which is outside the scope of this paper.

4.2. Lowering the Magnetic Field Strength

In the wind models presented in Paper I, we assumed the full magnetic field strength at $R = 3.5$ kpc of $7.8 \mu\text{G}$ (F01). It is certainly not clear that the entire inferred field strength (in the plane of the sky) would be present at the base of the wind, and evolve with the wind to high latitudes. In addition, if that magnetic field strength were lower, the synchrotron emission would of course also decrease, as $B^{(\gamma+1)/2} \sim B^{1.75}$ for $\gamma = 2.5$. To test this in the present work, we have decreased the magnetic field strength to $5.2 \mu\text{G}$, or 66% of the value used in Paper I; this is similar to the local magnetic-field strength. We are therefore assuming that only this portion of the synchrotron-derived magnetic field at $R = 3.5$ kpc is vertical field within the wind, and evolving with the wind to mid- and high-latitudes.

In passing, we point out that the magnetic field strengths presented in F01 are, in one sense, lower-limits to the field strength. We have found we are able to duplicate the results of the emissivity calculation in F01 by using the formulae for homogeneous fields perpendicular to the line of sight (see Ginzburg & Syrovatskii 1965), so that the calculated $7.8 \mu\text{G}$ magnetic field does not include the component of the field along the line of sight. On the other hand, it is important to note that the emissivity used in F01 is actually the lowest of the estimates of local emissivity in *Beuermann et al. (1985)* (as noted in F01), so it is not straightforward to estimate the uncertainty in the magnetic field towards the inner Galaxy.

In addition, it may be possible that the field in the wind is not strictly vertical, but rather helical (P. Biermann, private communication), as it may reasonably have a strong toroidal component due to shear in the Galactic disk. This would change the field strength in the plane of the sky, and thereby affect the synchrotron emission as a function of Galactic longitude. For simplicity, we neglect this effect in the current work.

4.3. Limiting the Effects of Uncertain Absorption

In the original fits in Paper I, we found the best-fit to the X-ray emission by calculating a χ^2 value throughout the entire latitude range of $b = -0^\circ$ to -90° . (We do not fit the emission in the Northern Galactic Hemisphere because of the more complex absorption and local emission sources, as discussed in Paper I.) However, the fit to the X-ray emission is strongly affected by absorption for $b \gtrsim -10^\circ$ and is dominated by the constant background components at $b \lesssim -40^\circ$. Intervening absorption was, and is, included in the models, but the distance to those absorbers is unknown, and so the absorption is calculated as a screen of material located between the observer and wind. This is perhaps a reasonable first assumption, but we can minimize the impact of that uncertainty in the fit by only calculating the χ^2 value between $-40^\circ < b < -10^\circ$, which we do for all of the following models. This also limits the impact of uncertainty in the stellar contribution to X-ray emission at low-latitudes (Masui et al. 2009; Revnivtsev et al. 2009), although such emission is more significant at higher energies. (In practice, we find that these modifications do not significantly change the parameters of the best-fit models in the previous or current work.)

4.4. Putting it All Together: an Improved Wind Model

Decreasing the wind model’s footprint, so that it stretches only from 3.5 to 4.5 kpc on the disk, and attempting a smaller magnetic-field strength ($B = 5.2 \mu\text{G}$) for the wind, we integrate the hydrodynamic equations for a range of initial (at the base of the wind) thermal-gas pressures, thermal gas densities, and z_{break} values to find the best-fit model (using the same methods of Paper I; see the Appendix) to reproduce the X-ray emission. This search entailed two large-scale searches through parameters space that integrated the hydrodynamic equations of motion for 13,475 models each. The first search spanned two orders of magnitude in thermal-gas density at the base of the wind, over one order of magnitude in thermal-gas pressures at the base of the wind, and z_{break} values spanning a factor of two (in 35, 35, and 11 steps, respectively), centered roughly near the best fit parameters from the wind model in Paper I. The best-fit to the soft X-ray emission from this scan was then input to a parameter-search of another 13,475 models distributed over a slightly smaller range in parameters (thermal-gas density ranging over a factor of ten, thermal-gas pressure ranging over a factor of 2.25, and z_{break} ranging over a factor about 1.5), to zoom in near the best fit. A final level of refinement in the parameter search was run to scan 1331 models in those three parameters (only varying each parameter by 40%, 20% and 20% around the previous best-fit value for $n_{\text{g},0}$, $P_{\text{g},0}$, and z_{break} , respectively).

The new best-fit model, found by this procedure, is shown in Figures 2 and 3, with the parameters for the fit given in Table 1. We also show the velocity and density profiles of this wind in Figures 4 and 5.

This model still improves on the static model of Almy et al. (2000) with respect to χ^2 . First, calculating χ^2 over the entire range of longitude ($-90^\circ < b < 0^\circ$, which is not the restricted region based on which the model was selected), the new model improves on the static polytrope’s χ^2 by a factor of 1.6 in the *ROSAT* ‘R4’ band and 2.1 in the ‘R5’ band. It is important to note that this fit is not as good as the original fit from Paper I, however: the new model overpredicts the emission in the X-ray ‘R4’ band by 15% at intermediate latitudes ($b \sim -30^\circ$), and slightly overpredicts the emission in

‘R5’ at low latitude ($l \sim -10^\circ$)⁵. (We note that this best-fit model is defined as the model with lowest χ^2 , calculated in the region from $-40^\circ < b < -10^\circ$ as defined in §4.3, but this only changes the best-fit model parameters by $\lesssim 3\%$ from the fit calculated with χ^2 defined over the entire latitude range.)

How have the changes in ΔR and B affected the wind model? In order to fit the X-ray emission while being launched from a thinner annulus, the gas density must increase at the base of the wind (here, by $\sim 30\%$). The gas pressure must increase as well, to keep the wind at approximately the same temperature (which is constrained by the relative emission in the ‘R4’ and ‘R5’ bands). The gas pressure has to increase still further for another reason, as well: as the magnetic-field strength has decreased and the density has increased, the power that is channeled from the cosmic rays to the gas also decreases (the power goes as $v_A \cdot \nabla P_{\text{cr}} \propto \frac{B}{\sqrt{\rho}} \cdot \nabla P_{\text{cr}}$). In the model of Paper I, energy from cosmic-rays played a significant role in heating the gas at mid-latitudes of $b \sim 15^\circ$. But, as B decreases and ρ increases, the power transmitted from the cosmic-ray component decreases, and the base gas temperature must increase still further to compensate (see Eq. A3 of the Appendix). This leads to an increase in the gas pressure at the base of the wind of approximately 104%. These are the dominant changes to the model as a result of the synchrotron constraints on the wind model.

Turning to other parameters of the model, the lengthscale for flow tube expansion (z_{break}) has decreased by $\sim 25\%$ (this parameter sets the scale-height for the expansion of the assumed flow tubes, and so, in a sense, represents an important set of assumptions about the magnetic geometry of the Galactic halo, which helps to define the acceleration profile). Meanwhile, the cosmic-ray pressure at the Galactic midplane has remained constant, by assumption. To further compare models, the mass outflow rate in this wind is $2.2 M_\odot/\text{yr}$ (very similar to the $2.1 M_\odot/\text{yr}$ for the previous model), and the terminal velocity is $\sim 570 \text{ km s}^{-1}$, significantly lower than the 760 km s^{-1} for the wind of Paper I. Overall, the model is somewhat similar to the past one in its ability to fit the X-ray emission, and in its parameter values, with the notable exception of strongly increased gas pressure. It is also important to point out that the initial velocity of gas in this simple wind model is 252 km s^{-1} ; such a high initial velocity is the result of our assumption that all of the energy is input as a delta function at the Galactic midplane, and so strongly indicates the need for a more detailed model of more gradual momentum and energy input to the wind.

Given this best-fit model to the soft X-ray emission, we can compute the synchrotron emission for the model. We compare the resultant brightness temperature to 408-MHz observations in Figure 6. This figure shows the averaged brightness temperature from the 408-MHz survey compared to the wind model outlined above (when all background and foreground sources have been added); both the data points and model curve are the result of an average over $-30^\circ < l < 30^\circ$. The wind model now successfully fits the observed synchrotron emission at the mid-latitudes of $-25^\circ < b < -10^\circ$.

⁵ It is important to stress that this assumes that the wind model plus backgrounds explains all of the X-ray emission observed towards the center of our Galaxy; it is very conceivable (*especially* now that the wind is much thinner than in Paper I) that other components may help explain the emission (such as the local ISM, the Galactic bulge, or even a bulge-related wind, see Tang et al. 2009), and therefore the requirements for the wind could be somewhat relaxed, and the strength of emission in the wind therefore decreased.

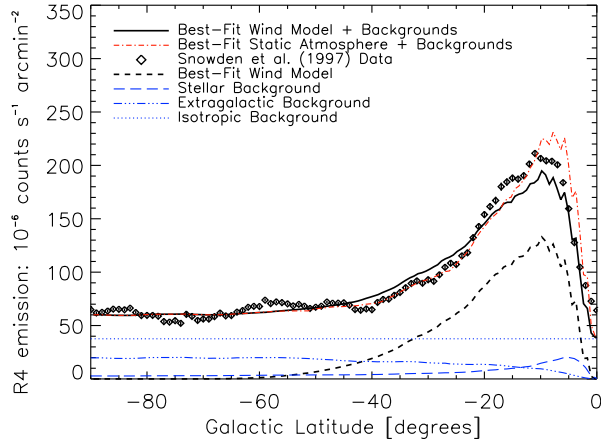


FIG. 2.— The best-fit model for a Galactic wind that stretches only between 3.5 and 4.5 kpc in Galactocentric radius with $B = 5.2 \mu\text{G}$; this comparison is for the ROSAT ‘R4’ band, centered roughly on 0.65 keV. The χ^2 for this fit is 2335 for 87 degrees of freedom, yielding a χ^2_ν of 26.8; this is slightly worse but comparable to the value of $\chi^2_\nu = 19.0$ from the best-fit R4 model in Paper I.

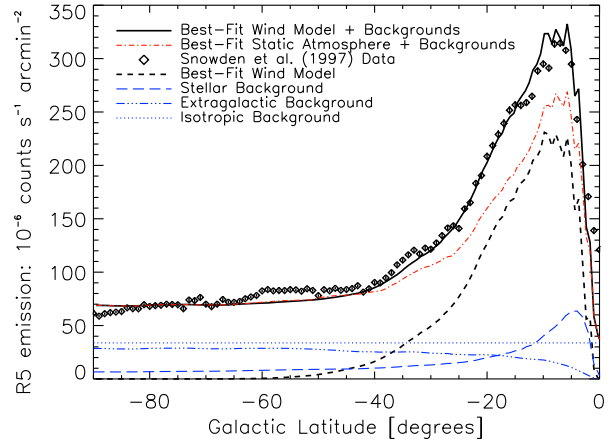


FIG. 3.— As in Figure 2, but for the ROSAT ‘R5’ band that is centered roughly on 0.85 keV. The χ^2 for this fit is 4522 with, again, 87 degrees of freedom; χ^2_ν is then 52.0, which again is only slightly worse fit than the $\chi^2_\nu = 48.9$ fit from Paper I.

We point out that this model fits simply due to the decreased ΔR and B ; as such, the model presented here is *not unique*: we have essentially modified the model to include more physically motivated launching conditions, finding a model that satisfies the observational requirements. There are, of course, a range of models that might also fit the observations, given corresponding changes in B and $P_{c,0}$: the range of possible models in this parameter space are shown in Figure 7. This figure displays the range of parameter values for $P_{c,0}$ and B for which winds are successfully launched; the color contours show the region of escaping winds with the colors encoding the χ^2 value for the fit to the two bands of soft X-ray emission, while the red lines show an estimate of the factor by which models in that parameter space would over- or under-predict the synchrotron emission: the red lines show the increase in synchrotron emission by a simple scaling of the best-fit synchrotron emission by $n_{\text{cr},e} \cdot B^{1.75}$. This figure shows the range of magnetic-field strengths and cosmic-ray pressures that would approximately satisfy the synchrotron (with the red line labeled ‘1.0’) and X-ray observations. The figure is also interesting in its own right, as it shows the wide range of magnetic-field strengths that can help to launch a wind. The biggest difference between the various models over the range of B is that the models with larger B can more easily reproduce the large scale-height of soft X-ray emission due to distributed heating by the cosmic-ray protons.

Note that we have added a constant foreground component (as well as other already known background sources, mentioned in §3.4) to our model in Figure 6. If the high-latitude emission is not local, the constraints on ΔR and B would be relaxed, and larger ΔR and B would be allowed.

This fit assumes that all other parameters are constant, to attempt to limit the number of variables. In particular, the cosmic-ray pressure at the base of the wind, $P_{c,0}$, has not been allowed to vary in any fits (although Fig. 7 displays the parameter space of $P_{c,0}$ and B_0 to show how joint variations affect synchrotron observations). In Figure 8, we show the parameter space where $P_{c,0}$ and $P_{g,0}$ are allowed to vary together;

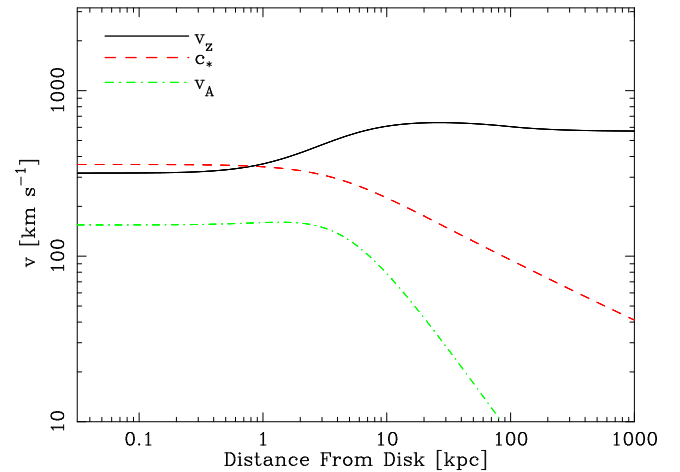


FIG. 4.— Velocity vs height for the best-fit model (parameters given in Table 1). The solid line shows the thermal-gas velocity within the wind, the dashed, red line shows the composite sound speed as a function of height, and the dot-dashed, green line shows the variation in Alfvén speed with height. The increase of velocity (even through the critical point, where $v = c_*$) is fairly standard, although this wind exhibits a slight decrease in velocity at large distances, as the increased wind radius encompasses more and more of the Galaxy’s mass.

TABLE 1
WIND PARAMETERS: NEW AND OLD

Parameter	New Value	Old Value	Fixed?
$P_{g,0}/k_B$	$4.0 \times 10^4 \text{ K cm}^{-3}$	$2.0 \times 10^4 \text{ K cm}^{-3}$	Varied
ρ_0	$9.0 \times 10^{-27} \text{ g cm}^{-3}$	$7.1 \times 10^{-27} \text{ g cm}^{-3}$	Varied
z_{break}	4.0 kpc	5.2 kpc	Varied
R_0 Range [Galactocentric]	3.5 to 4.5 kpc	1.5 to 4.5 kpc	Fixed
$P_{c,0}/k_B$	$2.2 \times 10^4 \text{ K cm}^{-3}$	$2.2 \times 10^4 \text{ K cm}^{-3}$	Fixed ^a
B_0	$5.2 \mu\text{G}$	$7.8 \mu\text{G}$	Fixed ^a
α	2.0	2.0	Fixed

^a Varied in Figure 7 only, and not fit to the data.

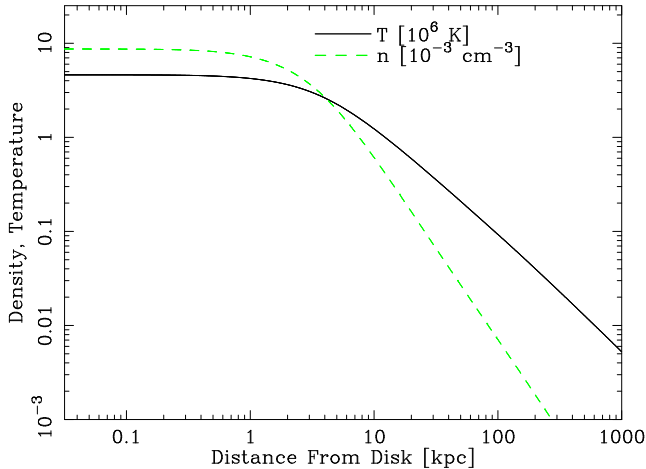


FIG. 5.— The temperature and density in the thermal gas as a function of height in the wind. The temperature is given by the solid, black line; as expected, as the wind accelerates and expands into the assumed flowtube, the temperature decreases. The temperature does not decrease as quickly as without cosmic-ray heating, however. Also in this plot, we show the particle-number density as a function of height with the dashed, green line.

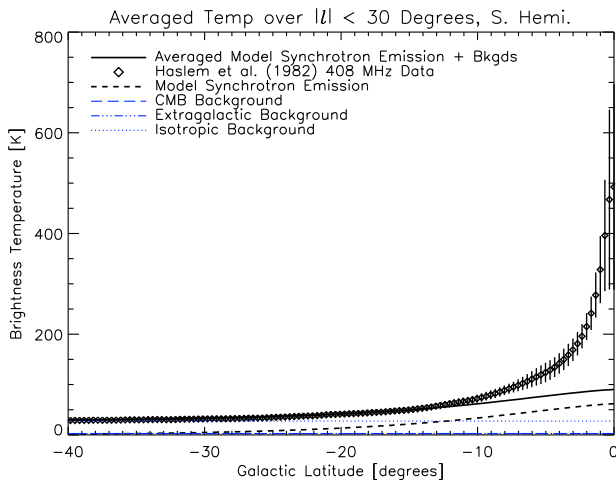


FIG. 6.— The integrated 408MHz synchrotron brightness temperature given by a wind that covers a smaller area on the Galactic disk than the model in Paper I; this wind extends only from 3.5kpc to 4.5kpc on the disk, and has $B = 5.2\mu\text{G}$.

this plot shows the importance of adding cosmic-ray pressure: the area of allowed winds (shown by the color contours) increases markedly for $P_{c,0} > 10^4 \text{ cm}^{-3} \text{ K}$. In that regime, Galactic winds exist for lower thermal pressures than would otherwise be allowed. This plot also shows the best fit (from Table 1); however, interestingly, when $P_{c,0}$ is allowed to ‘float’, a fit is preferred where $P_{c,0}$ and $P_{g,0}$ are approximately equal. However, this results in a cosmic-ray electron density that, given our stated assumptions about the ratio of the cosmic-ray electron-to-proton fraction (§3.1) and other parameters in the fit, would violate the radio-synchrotron constrains. Of course, if the proton-to-electron ratio was 100:1 instead of 50:1, as assumed here, that would relax this constraint on the wind greatly.

Finally, in Figure 9, we show the allowed winds as a func-

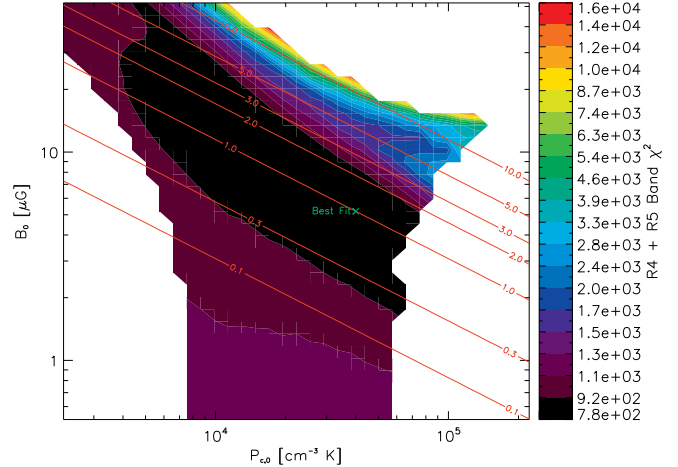


FIG. 7.— The parameter space of the best-fitting model as a function of the magnetic-field strength at the base of the wind, B_0 , and the cosmic-ray pressure at the base of the wind, $P_{c,0}$. The color-contour-delineated region denotes those winds which can be launched from the Galactic potential, and the color contours show the combined, total χ^2 for fitting the X-ray emission in the ROSAT ‘R4’ and ‘R5’ bands. The labeled red lines indicate the trend of synchrotron emission *above* that observed in the best-fitting model. One can see a range of models with radio emission of the level of that observed (the red line marked ‘1.0’) with relatively low χ^2 values. The best-fit model to the soft X-ray observations (with $P_{c,0}$ fixed) is indicated by the green ‘x’. **NB:** The red lines here give the synchrotron scaling of $I_\nu \propto n_{\text{cr},e} B^{1.75}$ appropriate for $\gamma = 2.5$, and **do not** represent the results of a set of synchrotron simulations, which would yield modified curves due to variations in wind acceleration profiles impacting the run of density with height. For winds in this survey, the parameters $P_{g,0}$, n_0 , z_{break} and α were held fixed.

tion of the wind parameters n_0 and $P_{g,0}$. This figure is much like the corresponding Figure 10 in Paper I, albeit with a ‘slimmer’ region of allowed winds due to the increased importance of gas pressure vs. cosmic-ray pressure in the newer model (due to the smaller magnetic-field strength).

4.5. Another Diagnostic: the Wind’s Brightness Temperature Spectral Index

There is another possible constraint on the wind from synchrotron observations: the temperature spectral index. After much remarkable work on survey and survey calibrations over the last few decades (e.g., Haslam et al. 1982; Reich 1982; Reich & Reich 1986; Reich et al. 2001), maps exist of the synchrotron spectral index over the sky (Reich & Reich 1988a,b; Reich et al. 2004). In preparation for a new analysis of the spectral index (some early results have already appeared in Reich et al. 2004), we can make predictions of the temperature spectral indices that would be produced by the wind. We calculate the brightness temperature spectral index from predicted 408MHz and 1420MHz. This spectral index is defined as:

$$\beta = -\frac{\log(T(\nu_2)/T(\nu_1))}{\log(\nu_2/\nu_1)}, \quad (13)$$

where for this analysis, $\nu_1 = 408 \text{ MHz}$ and $\nu_2 = 1420 \text{ MHz}$. As in the case of total intensity, we calculate this temperature spectral index for the average emission in the model and in the data for $l = 0^\circ$, and over the range of latitude where the wind emission seems to dominate the observed emission, $10^\circ < |b| < 25^\circ$ (and also, where discrete sources are much less numerous). For a similar region, Reich et al. (2004)

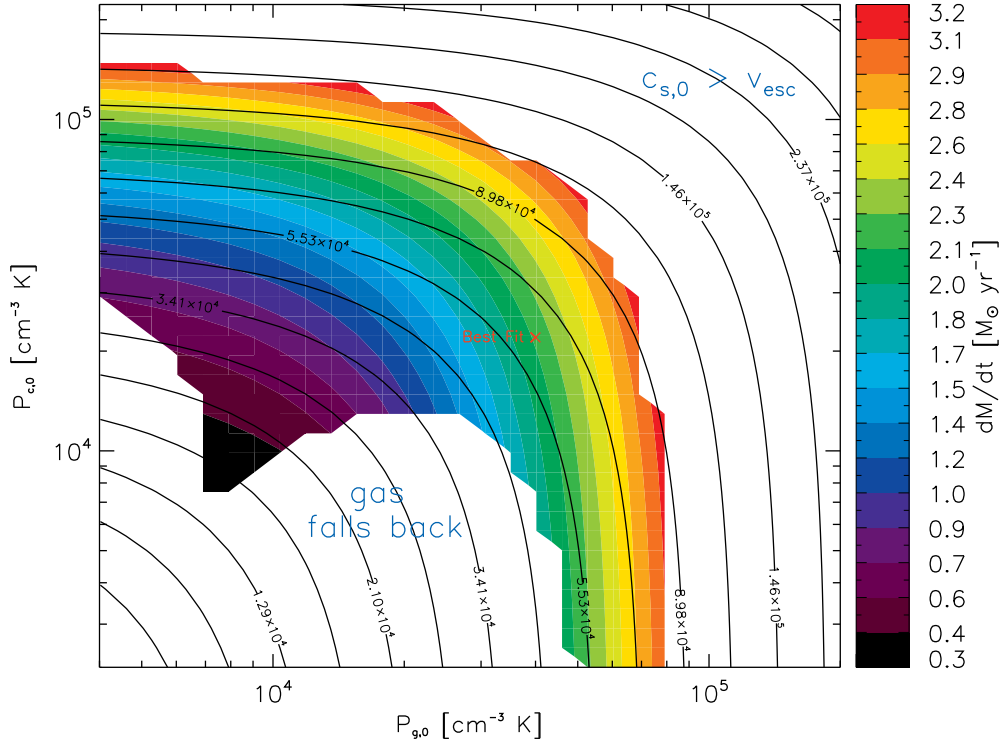


FIG. 8.— The parameter space of successful outflows as a function of gas pressure at the base of the wind, $P_{g,0}$, and cosmic-ray pressure at the base of the wind, $P_{c,0}$. The color contours outline the region of allowed winds, with the color code specifying the mass outflow rate in the wind. However, in this figure, the black lines denote the total pressure in the wind (cosmic-ray pressure plus thermal pressure). As expected, the mass outflow rate generally increases with total pressure in the wind. This figure also shows the important role played by cosmic-ray pressure, though: cosmic-ray pressure above $P_{c,0} \sim 10^5 \text{ cm}^{-3} \text{ K}$ result in successful winds for values of $P_{g,0}$ that would ordinarily not allow outflows. For winds in this survey, the parameters n_0 , B_0 , z_{break} and α were held fixed.

found the temperature spectral index $\beta \sim 2.65$ at $b \sim 30^\circ$ (see their Fig. 3; this measurement includes all components along the line of sight).

The temperature spectral index for the best-fit wind model (alone) is shown as the solid line in Figure 10. When we consider the spectral index of the wind (without the foreground emission component accounted for), the wind spectral index gradually steepens, as expected for the cooling cosmic-ray electron population: the wind model has $\beta \sim 2.85$ at $b = 10^\circ$, rising to $\beta \sim 3.1$ by $b = 40^\circ$. This is significantly steeper than the spectral indices seen in Reich et al. (2004), which approximately span the range of 3.0 to 2.6, *falling* with height above the disk.

This source of “flattening” of the observed synchrotron spectral index has been the source of some debate (e.g., Reich & Reich 1988a; Pohl & Schlickeiser 1990). In this debate, we would like to emphasize the importance of *multiple emission components* that may lie along the line of sight (as also mentioned in Pohl & Schlickeiser 1990). Our model (when considered alone) clearly shows a steepening of the spectral index with height, but when we calculate the spectral index of the wind plus a constant (again, perhaps local) foreground, we find a nearly constant spectral index; this is shown by the dashed line in Figure 10. We note that this is the simplest foreground possible, but it is sufficient to significantly change the run of spectral index with height.

As such, until we have a more detailed understanding of background and foreground synchrotron sources, it will be difficult to draw definitive conclusions about any one com-

ponent. What is of course needed here is an improved understanding of the nature of the various components and how they work together, in order to constrain the various physical processes and dynamics of our Galaxy (Strong et al. 2004a; Cox 2005).

5. RESULTS & DISCUSSION

We have continued to build on the results of previous work, and on our own Paper I, by applying radio-synchrotron constraints derived from the 408MHz all-sky survey of Haslam et al. (1982) to our cosmic-ray and thermal-gas pressure driven wind model. The original model of Paper I overpredicts mid-latitude synchrotron radiation (although it would approximately reproduce the observations if a cosmic-ray proton-to-electron ratio of 100:1 was adopted; we retain the locally observed ratio of approximately 50:1 to place the most stringent constraint on the wind model). However, a wind model can be found that is consistent with the observations and with more physically-plausible launch conditions, such as a thinner wind with $\Delta R \sim 1 \text{ kpc}$ and with smaller $B \sim 5 \mu\text{G}$.

Both the trend of star formation with Galactocentric radius and radio-synchrotron observations point to a wind that is launched from a smaller “footprint” than hypothesized in Paper I. This range of radii seems plausible if we envision the wind as launched from within the inner spiral arm, or the inner molecular ring, which has been observed in this radius range. We also found that a smaller magnetic field strength was required: the vertical field in the wind can be decreased from

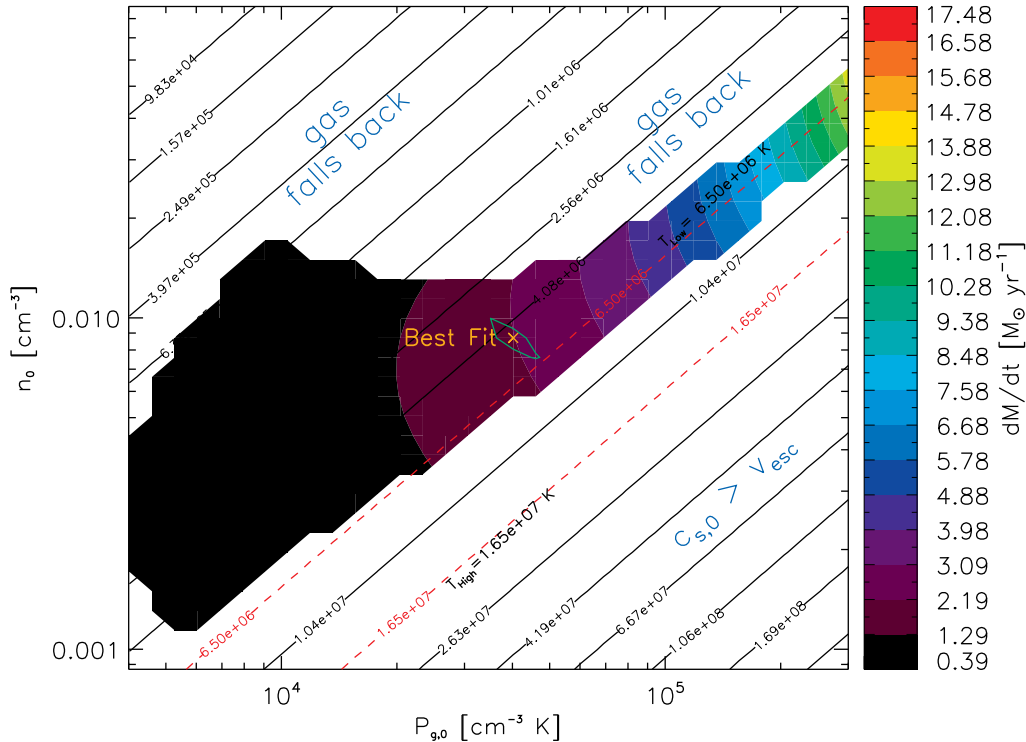


FIG. 9.— The parameter space of allowed models as a function of gas pressure at the base of the wind, $P_{g,0}$ and density, n_0 . The color contours show the range of models where plasma escapes the Galaxy, with the color corresponding to the mass outflow rate, given in the color bar on the right. The solid lines are marked with the gas temperature along that line; the red-dashed line give the lower (T_{low}) and upper (T_{high}) limits for the gas temperature of a purely thermally-driven Galactic wind. The best fit is shown with the yellow ‘x’, surrounded by the region where $\chi^2 < 2 \cdot \chi_{\text{min}}^2$, giving an indication of the region of minimally acceptable fits to the X-ray emission. Compared to the similar figure in Paper I (that paper’s Fig. 10), the region of allowed winds is smaller at higher pressure due to the relative dominance of gas pressure in this winds. For winds in this survey, the parameters $P_{c,0}$, B_0 , z_{break} and α were held fixed.

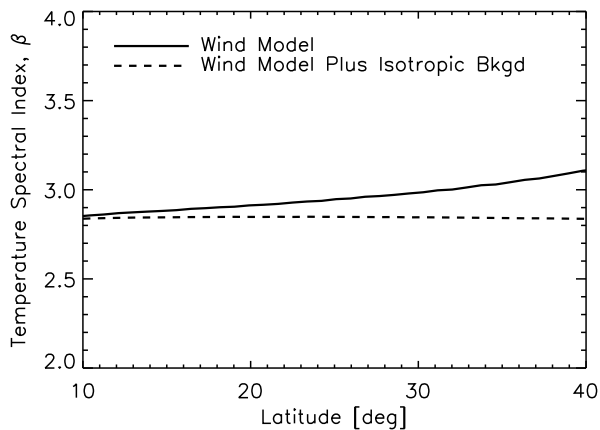


FIG. 10.— The temperature spectral index, β , for the Galactic wind model along $l = 0^\circ$. The solid line shows the trace of the spectral index for the wind model alone, while the dashed line gives the spectral index for the wind with a foreground emission component.

$7.8\mu\text{G}$ to $5.2\mu\text{G}$ and fit the observations. The resulting wind model predicts a level of synchrotron emission that agrees with the level observed at high latitude, does not overpredict synchrotron emission at low- to mid-latitudes ($b \sim -15^\circ$), and reproduces the X-ray emission in the *ROSAT* ‘R4’ and ‘R5’ bands. However, the fit in the ‘R4’ band, while still improv-

ing on previous static models, does not fit as well as model in Paper I. We have suggested that this may be due to the lack, in this model, of X-ray emission from static gas. Still, the constraint of the synchrotron emission requires that the wind have a smaller radial extent, and have a smaller magnetic field; the ‘best-fit’ model, in this paper, represents the best agreement between these two different constraints (while keeping $P_{c,0}$ constant).

While comparing the synchrotron observations to the wind model, we have found that a significant fraction of high-latitude ($b < -40^\circ$) synchrotron radiation is consistent with a local source rather than Galactic-halo emission. This is in agreement with other work (see, e.g. Sun et al. 2008, and references therein), and hints that the synchrotron halo model of Beuermann et al. (1985) is perhaps a significant over-estimate of the actual Galactic halo. As the model of Beuermann et al. (1985) is still in widespread use, this seems an important point to stress. We include this local emission to again strongly constrain this Galactic wind model, to see if it can survive. It appears that it can.

Choosing this wind model has other implications for the effect of a wind on the Galactic central region. We wish to point out, however, that we do not consider the diffusion of electrons throughout the Galaxy; only the vertical advection of cosmic rays within a small range of Galactocentric radii is considered. Given this small range of launching radii, and since the radial diffusion rate of cosmic-rays is much less than the vertical advection rate, the present wind model would not

advect cosmic rays from a widespread range of Galactocentric radii. Indeed, we envision that, since cosmic rays stream mostly along magnetic field lines, this wind's advection of cosmic rays would not impact the cosmic-ray distribution in the solar neighborhood.

This advection of cosmic rays from the Galactic midplane could have other effects, though: in Paper I, it was hypothesized that such a wind could help evacuate cosmic rays from the central Galactic disk where γ -ray observations seem to indicate that cosmic-ray protons are not as abundant as the apparent supernova rate in that region of the Galaxy would suggest (Bloemen 1989; Bloemen et al. 1993; Breitschwerdt et al. 2002). This type of wind and its effect on the cosmic-ray population has been studied in more detail by Gebauer & de Boer (2009). The relative dearth of cosmic rays towards the center of the Galaxy might then require an additional component, such as a significant change in the $W_{\text{CO-to-}N(\text{H}_2)}$ factor, as suggested by Strong et al. (2004b). This model will also require more localized supernova power to launch the wind. In the wind model presented in Paper I, the wind required approximately 2.1 times the supernova power that is observationally inferred in the radial range beneath it ($R = 1.5$ to 4.5 kpc), using the estimate of the supernova rate as a function of R in F01. Using the same method, the wind model presented in this paper requires approximately 2.7 times the supernova power in the $\Delta R = 1$ kpc range of radii that it is launched from, assuming that each supernova produces $10^{51} \text{ erg s}^{-1}$ (using instead the supernova rates vs R of McKee & Williams 1997, the wind requires 1.9 times the estimated supernova power). While, as mentioned in Paper I, thermal conduction and clumping of the outflowing gas may help reduce this estimate, this calculation shows that the synchrotron data has perhaps pushed the simple wind model to the limit of its applicability to the Galaxy. However, this estimate is also very dependent on the radial distribution of supernovae; if uncertainties in the distances to supernovae are artificially spreading out the distribution of supernovae, then the power in the Molecular Ring may be underestimated. All

of these considerations point to the need for not only a more complete model but also for continued comparisons of the model with other observations.

Overall, this paper has shown that the wind model can satisfy both the synchrotron observations and can be made more compatible with what is already known of Galactic structure. This work satisfies those observations and constraints by limiting the radial extent of the wind and magnetic field strength within the wind. The most direct way to continue testing the model is to produce γ -ray predictions, and compare those predictions with *Fermi*/LAT observations of the diffuse Galactic γ -ray emission.

6. ACKNOWLEDGMENTS

The authors would like to thank T. Porter, A. Strong, and their collaborators for their work on their representation of the Interstellar Radiation Field, and for making their map of the ISRF available online. The authors also would like to thank Bob Benjamin, Dieter Breitschwerdt, Katia Ferriere, Bryan Gaensler, Amanda Kepley, Dan McCammon, Justin Morgan, Peter Biermann, Wolfgang Reich, Blair Savage, and Eric Wilcots for questions and helpful conversation. The authors also thank the referee for comments that improved the paper.

Portions of the analysis presented here made use of the Perl Data Language (PDL) developed by K. Glazebrook, J. Brinchmann, J. Cerney, C. DeForest, D. Hunt, T. Jenness, T. Luka, R. Schwebel, and C. Soeller and can be obtained from <http://pdl.perl.org>. PDL provides a high-level numerical functionality for the Perl scripting language (Glazebrook & Economou 1997).

This work was supported by NSF AST-0507367, NSF AST-0907837, and NSF PHY-0215581 & NSF PHY-0821899 (to the Center for Magnetic Self-Organization in Laboratory and Astrophysical Plasmas). This research has made use of NASA's Astrophysics Data System.

APPENDIX

WIND MODEL EQUATIONS

For completeness, we review here the equations for the cosmic-ray and thermal-gas pressure driven wind from Everett et al. (2008); please refer to that paper for further details.

Our wind model builds on the equations first presented by Breitschwerdt et al. (1991) and Breitschwerdt et al. (1993). This model is a 1D, semi-analytic model that treats both the thermal gas and cosmic-ray components as fluids. The development of the outflow with height is governed by the equation of mass conservation (assuming no mass is added as the wind flows out of the Galactic plane):

$$\frac{d}{ds}(\rho v A) = 0 \quad (\text{A1})$$

where ρ is the gas mass density, z is the height above the Galactic plane, and A is the cross sectional area of the wind. Since this is a 1D system of equations, we must prescribe the cross-sectional area as a function of height:

$$A(z) = A_0 \left[1 + \left(\frac{z}{z_{\text{break}}} \right)^\alpha \right] \quad (\text{A2})$$

where A_0 is cross-sectional area of the flowtube at the Galactic midplane, and α is the power-law governing the divergence of the flowtube; the flowtube has a roughly constant cross section $A \sim A_0$ until approximately the height z_{break} , where the area increases as z^α . We chose $\alpha = 2$ to mimic a spherical divergence with height above z_{break} and leave z_{break} as a parameter in our fitting process, as its value is not known beforehand.

The thermal-gas and cosmic-ray pressure change with height via the relations:

$$\frac{dP_g}{dz} = \left(c_g^2 - \gamma_c(\gamma_g - 1) \frac{P_c}{\rho} \frac{1}{M_A} \frac{M_A + \frac{1}{2}}{M_A + 1} \right) \frac{d\rho}{dz}, \quad (\text{A3})$$

$$\text{and } \frac{dP_c}{dz} = \frac{\gamma_c P_c M_A + \frac{1}{2} d\rho}{\rho M_A + 1} \frac{d\rho}{dz}, \quad (\text{A4})$$

where P_g and P_c are the thermal-gas and cosmic-ray pressures, c_g is the speed of sound, γ_g and γ_c are the polytropic indices for the thermal gas and cosmic rays (set to 5/3 and 4/3, respectively), and $M_A = v/v_A$ is the Alfvén Mach number for the gas (v is the velocity of the gas and v_A is the Alfvén speed).

The magnetic-field strength evolves with height by requiring that the magnetic flux remains constant; hence, $B(z)A(z) = [\text{constant}]$. We note that the magnetic field is important here not as a direct source of pressure or tension, but as a “conduit” of sorts, through which the cosmic rays communicate momentum and energy to the thermal gas. This is why we require a vertical magnetic field; a magnetic-field component must lie along the direction of the cosmic-ray pressure gradient in order to excite the streaming instability (e.g., Wentzel 1968; Kulsrud & Pearce 1969; Breitschwerdt et al. 1991).

The terms in these equations (Eq. A3 and A4) can be understood as follows. The first term in Equation A3 describes how the gas pressure changes due to expansion and acceleration of the gas in the flowtube. The second term in Equation A3 couples the cosmic-ray pressure to the gas pressure; this term represents the damping of cosmic-ray generated Alfvén waves which then heat the gas and help drive the wind. This type of immediate wave damping is important as rapid wave-damping mechanisms are known to occur in the ISM, and this also limits the growth of the Alfvén waves such that the perturbation in magnetic-field strength remains below the background field strength. This idea was first introduced (but not yet widely used, since the Alfvén wave growth was small below the critical point) in Breitschwerdt et al. (1991) and was also used in Zirakashvili et al. (1996) and Ptuskin et al. (1997); we discuss this in more detail in §2 of Paper I. Finally, Equation A4 describes the loss in cosmic-ray pressure due to adiabatic expansion, wave momentum transport to the gas, and to wave generation by the cosmic rays.

The velocity of gas in the wind is derived by solving the wind equation, which we write as:

$$\rho v \frac{dv}{dz} + c_*^2 \frac{d\rho}{dz} = -\rho g. \quad (\text{A5})$$

This equation of motion is much like the equation of motion for models that rely only on thermal-gas pressure, except that instead of a gas sound speed, c_g , we use c_* , which gives a “composite sound speed” (see Breitschwerdt et al. 1991), defined as:

$$c_*^2 = \frac{d(P_g + P_c)}{d\rho} \quad (\text{A6})$$

where P_g and P_c were given in Equations A3 and A4.

To solve for the functions $v(z)$, $\rho(z)$, $P_g(z)$, $P_c(z)$ and $B(z)$, we must integrate the above equations from the Galactic midplane to a distance far above the galactic midplane, correctly threading the critical point that occurs when $v = c_*$. When starting the integrations from the midplane, we set (from other models and observations) and fix the value of the midplane cosmic-ray pressure, the magnetic field strength, and the power-law α that governs the opening of the flowtube cross-sectional area (see Table 1 for values). We do not have strong constraints on the values of the midplane thermal-gas pressure, the hot-gas midplane density, and the height where the flowtube starts to rapidly expand (z_{break}) so we leave those as free parameters which are then constrained by the soft X-ray and radio observations. These parameters are also considered in some detail in Paper I and in §2.

REFERENCES

- Abramowitz, M., & Stegun, I. A. 1972, *Handbook of Mathematical Functions*, ed. M. Abramowitz & I. A. Stegun
- Almy, R. C., McCammon, D., Digel, S. W., Bronfman, L., & May, J. 2000, *ApJ*, 545, 290
- Beck, R. 2001, *Space Science Reviews*, 99, 243
- Beuermann, K., Kanbach, G., & Berkhuijsen, E. M. 1985, *A&A*, 153, 17
- Binney, J. 2009, in *IAU Symposium*, Vol. 254, *IAU Symposium*, ed. J. Andersen, J. Bland-Hawthorn, & B. Nordström, 145–152
- Bland-Hawthorn, J., & Cohen, M. 2003, *ApJ*, 582, 246
- Bloemen, H. 1989, *ARA&A*, 27, 469
- Bloemen, H. 1991, in *ASP Conf. Ser. 18: The Interpretation of Modern Synthesis Observations of Spiral Galaxies*, ed. N. Duric & P. C. Crane, 27–36
- Bloemen, J. B. G. M., Dogiel, V. A., Dorman, V. L., & Ptuskin, V. S. 1993, *A&A*, 267, 372
- Breitschwerdt, D. 2003, in *Revista Mexicana de Astronomía y Astrofísica Conference Series*, ed. J. Arthur & W. J. Henney, 311–316
- Breitschwerdt, D., Dogiel, V. A., & Völk, H. J. 2002, *A&A*, 385, 216
- Breitschwerdt, D., McKenzie, J. F., & Völk, H. J. 1991, *A&A*, 245, 79 (BMV91)
- , 1993, *A&A*, 269, 54
- Breitschwerdt, D., & Schmutzler, T. 1994, *Nature*, 371, 774
- Breitschwerdt, D., Völk, H. J., & McKenzie, J. F. 1987, in *Interstellar Magnetic Fields: Observation and Theory*, ed. R. Beck & R. Graeve, 131–141
- Broadbent, A., Haslam, T. C. G., & Osborne, L. J. 1990, in *International Cosmic Ray Conference*, Vol. 3, *International Cosmic Ray Conference*, 229–
- Cox, D. P. 2005, *ARA&A*, 43, 337
- de Oliveira-Costa, A., Tegmark, M., Gaensler, B. M., Jonas, J., Landecker, T. L., & Reich, P. 2008, *MNRAS*, 388, 247
- Duric, N. 1990, in *IAU Symposium*, Vol. 140, *Galactic and Intergalactic Magnetic Fields*, ed. R. Beck, R. Wielebinski, & P. P. Kronberg, 235–
- Everett, J. E., Zweibel, E. G., Benjamin, R. A., McCammon, D., Rocks, L., & Gallagher, III, J. S. 2008, *ApJ*, 674, 258, **Paper I**
- Ferrière, K. M. 2001, *Reviews of Modern Physics*, 73, 1031, **F01**
- Fleishman, G. D., & Tokarev, Y. V. 1995, *A&A*, 293, 565
- Gebauer, I., & de Boer, W. 2009, *ArXiv e-prints*
- Ginzburg, V. L., & Syrovatskii, S. I. 1965, *ARA&A*, 3, 297
- Glazebrook, K., & Economou, F. 1997, *Dr. Dobb’s Journal*, 9719, 45
- Haslam, C. G. T., Salter, C. J., Stoffel, H., & Wilson, W. E. 1982, *A&AS*, 47, 1
- Heiles, C. 1996, in *Astronomical Society of the Pacific Conference Series*, Vol. 97, *Polarimetry of the Interstellar Medium*, ed. W. G. Roberge & D. C. B. Whittet, 457–
- Ipavich, F. M. 1975, *ApJ*, 196, 107
- Jackson, J. M., Rathborne, J. M., Shah, R. Y., Simon, R., Bania, T. M., Clemens, D. P., Chambers, E. T., Johnson, A. M., Dormody, M., Lavoie, R., & Heyer, M. H. 2006, *ApJS*, 163, 145
- Jokipii, J. R., & Morfill, G. 1987, *ApJ*, 312, 170
- Kulsrud, R., & Pearce, W. P. 1969, *ApJ*, 156, 445
- Kulsrud, R. M., & Cesarsky, C. J. 1971, *Astrophys. Lett.*, 8, 189
- Lerche, I., & Schlickeiser, R. 1982, *A&A*, 107, 148
- Masui, K., Mitsuda, K., Yamasaki, N. Y., Takei, Y., Kimura, S., Yoshino, T., & McCammon, D. 2009, *PASJ*, 61, 115
- McKee, C. F., & Williams, J. P. 1997, *ApJ*, 476, 144
- Moskalenko, I. V., & Strong, A. W. 2000, *ApJ*, 528, 357
- Park, S., Finley, J. P., & Dame, T. M. 1998, *ApJ*, 509, 203
- Park, S., Finley, J. P., Snowden, S. L., & Dame, T. M. 1997, *ApJ*, 476, L77+
- Pohl, M. 1993, *A&A*, 279, L17
- Pohl, M., & Schlickeiser, R. 1990, *A&A*, 239, 424
- Porter, T. A., & et al. 2005, in *International Cosmic Ray Conference*, Vol. 4, *International Cosmic Ray Conference*, 77–
- Porter, T. A., Moskalenko, I. V., Strong, A. W., Orlando, E., & Bouchet, L. 2008, *ApJ*, 682, 400

- Ptuskin, V. S., Völk, H. J., Zirakashvili, V. N., & Breitschwerdt, D. 1997, *A&A*, 321, 434
- Reich, P., & Reich, W. 1986, *A&AS*, 63, 205
- , 1988a, *A&A*, 196, 211
- , 1988b, *A&AS*, 74, 7
- Reich, P., Reich, W., & Testori, J. C. 2004, in *The Magnetized Interstellar Medium*, ed. B. Uyaniker, W. Reich, & R. Wielebinski, 63–68
- Reich, P., Testori, J. C., & Reich, W. 2001, *A&A*, 376, 861
- Reich, W. 1982, *A&AS*, 48, 219
- Reich, W., & Reich, P. 2008, *ArXiv e-prints*
- Revnivtsev, M., Sazonov, S., Churazov, E., Forman, W., Vikhlinin, A., & Sunyaev, R. 2009, *Nature*, 458, 1142
- Roger, R. S., Costain, C. H., Landecker, T. L., & Swerdlyk, C. M. 1999, *A&AS*, 137, 7
- Skilling, J. 1975, *MNRAS*, 172, 557
- Snowden, S. L., Egger, R., Freyberg, M. J., McCammon, D., Plucinsky, P. P., Sanders, W. T., Schmitt, J. H. M. M., Truemper, J., & Voges, W. 1997, *ApJ*, 485, 125
- Snowden, S. L., Freyberg, M. J., Plucinsky, P. P., Schmitt, J. H. M. M., Truemper, J., Voges, W., Edgar, R. J., McCammon, D., & Sanders, W. T. 1995, *ApJ*, 454, 643
- Strong, A. W., & Moskalenko, I. V. 1998, *ApJ*, 509, 212
- Strong, A. W., Moskalenko, I. V., & Reimer, O. 2000, *ApJ*, 537, 763
- , 2004a, *ApJ*, 613, 962
- Strong, A. W., Moskalenko, I. V., Reimer, O., Digel, S., & Diehl, R. 2004b, *A&A*, 422, L47
- Sun, X. H., Reich, W., Waelkens, A., & EnBlin, T. A. 2008, *A&A*, 477, 573
- Tang, S., Wang, Q. D., Mac Low, M.-M., & Joung, M. R. 2009, *ArXiv e-prints*
- Veilleux, S., Cecil, G., & Bland-Hawthorn, J. 2005, *ARA&A*, 43, 769
- Waelkens, A., Jaffe, T., Reinecke, M., Kitaura, F. S., & EnBlin, T. A. 2009, *A&A*, 495, 697
- Webber, W. R. 1983, in *NATO ASIC Proc. 107: Composition and Origin of Cosmic Rays*, ed. M. M. Shapiro, 83–100
- Webber, W. R. 1998, *ApJ*, 506, 329
- Wentzel, D. G. 1968, *ApJ*, 152, 987
- Wolleben, M. 2007, *ApJ*, 664, 349
- Zirakashvili, V. N., Breitschwerdt, D., Ptuskin, V. S., & Völk, H. J. 1996, *A&A*, 311, 113
- Zirakashvili, V. N., & Völk, H. J. 2006, *ApJ*, 636, 140
- Zweibel, E. G., & Heiles, C. 1997, *Nature*, 385, 131